Modal Analysis: the International Journal of Analytical and Experimental Modal Analysis v 8 n 1 Jan 1983 p 45-54

STINGER MASS COMPENSATION PROBLEMS: EXPERIMENTAL INVESTIGATION

by X. Hu and K.G. McConnell, Iowa State University

ABSTRACT

Stinger mass compensation problems are investigated experimentally for the case when the load cell is mounted on the stinger's exciter end. Two test cases are performed experimentally using three different mass compensation methods. The first test uses a rigid mass specimen while the second uses a double cantilever beam specimen. The experimental results show that the measured frequency response function (FRF) can be underestimated if mass compensation is based on the stinger exciter–end acceleration and can be overestimated if the mass compensation is based on the structure–end acceleration because of the stinger's compliance. The mass compensation that is based on two accelerations is seen to improve the accuracy considerably. However, experimental difficulties have been found in predicting the resonant magnitude for all three mass compensation methods.

List of Symbols

a_1	stinger's exciter–end acceleration
a_2	stinger's structure–end acceleration
F_{c1}	measured force acting on the test structure by using mass compensation based on a_1
F_{c2}	measured force acting on the test structure by using mass compensation based on a_2
F_{c12}	measured force acting on the test structure by using mass compensation based on both a_1 and a_2
F_m	measured force by force transducer
$H_{c1}(\omega)$	measured structure's accelerance after mass compensation based on a_1
$H_{c2}(\omega)$	measured structure's accelerance after mass compensation based on a_2
$H_{c12}(\omega)$	measured structure's accelerance after mass compensation based on both a_1 and a_2
H_s	structure's driving point accelerance without stinger
m_1	effective end mass mounted on the stinger's exciter end
m_2	effective end mass mounted on the stinger's structure end
m_r	stinger's mass

Dr. Ximing Hu, Visiting Scientist and Kenneth G. McConnell (Fellow of SEM), Professor, Dept. of Aerospace Engineering and Engineering Mechanics, Iowa State University, Ames, Iowa 50011

Final manuscript received: July 14, 1992

1. Introduction

The stinger's mass compensation problems are discussed theoretically in Part One [1] where the results show that the stinger's compliance causes mass compensation errors. These errors can not be neglected in the high frequency regions if the mass compensation is based on one acceleration (stinger's structure–end or exciter–end acceleration). Mass compensation based on two accelerations has been shown to reduce these errors considerably.

In this paper, the stinger mass compensation problems are investigated experimentally. Two tests were performed to substantiate both the theoretical results and the new mass compensation method's effectiveness. The first experiment uses a rigid–mass specimen while the second experiment uses a double cantilever beam specimen.

2 Three Mass Compensation Methods

Figure 1 shows a complete accelerance measurement setup with the force transducer mounted on the stinger's exciter end. Part of the exciter's output force is required to accelerate the effective end mass ($m_1 + m_r + m_2$) between the force transducer's sensor and the test structure. This part of the force can be removed by subtracting a signal that is proportional to the effective end mass's acceleration from the the force transducer's signal to obtain the force acting on the structure under test. In this experimental work, mass compensation is implemented digitally on the basis of three different acceleration sets.

(1) Mass compensation based on a_1

If we assume m_1, m_r, and m_2 have the same acceleration a_1, then we obtain

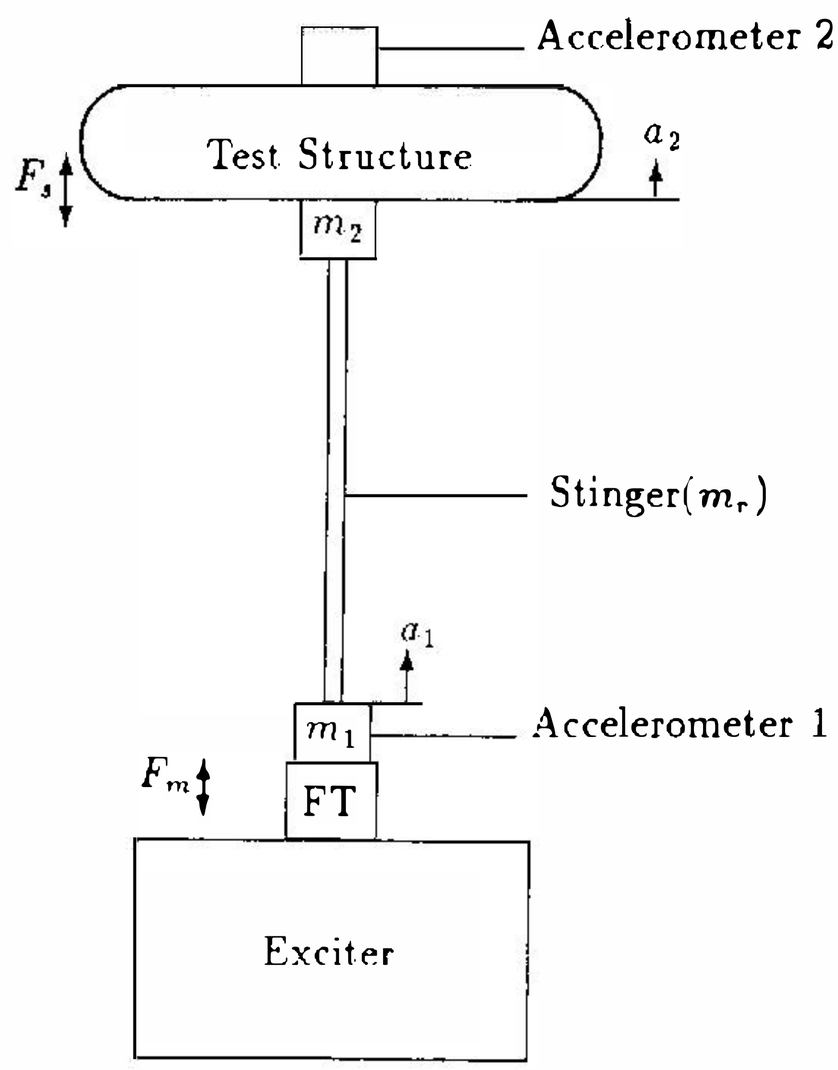

Fig. 1 Mobility measurement with force transducer at the stinger's exciter end

$$F_{c1} = F_m - (m_1 + m_r + m_2)a_1 \tag{1}$$

and

$$H_{c1}(\omega) = \frac{a_2}{F_{c1}} \tag{2}$$

(2) Mass compensation based on a_2

Now if we assume m_1, m_r, and m_2 have the same acceleration a_2, then the correct force after mass compensation becomes

$$F_{c2} = F_m - (m_1 + m_r + m_2)a_2 \tag{3}$$

and the measured accelerance becomes

$$H_{c2} = \frac{a_2}{F_{c2}} \tag{4}$$

(3) Mass compensation based on both a_1 and a_2

The proposed mass compensation method uses both accelerations a_1 and a_2 where a_1 is used with m_1 and half of the stinger's mass ($m_r/2$) while a_2 is used with mass m_2 and the other half of the stinger's mass.

$$F_{c12} = F_m - \left(m_1 + \frac{m_r}{2}\right)a_1 - \left(\frac{m_r}{2} + m_2\right)a_2 \tag{5}$$

$$H_{c12} = \frac{a_2}{F_{c12}} \tag{6}$$

3. Test Equipment and Instrumentation

An electodynamic shaker is used to excite the structure. A control unit and a power amplifier are used to control and drive the shaker. The primary quantities to be measured during a test are the driving force, the exciter table acceleration, and the structure's driving point acceleration. The structure's driving point acceleration is measured by a piezoelectric accelerometer. A Kistler model 808T accelerometer is chosen to measure the force transducer's base acceleration because of its design to carry axial loads. The driving force is measured by a piezoelectric force transducer. The output signal of each transducer is fed through either a charge amplifier or an interface power unit to a digital processing oscilloscope that is used to perform data acquisition, digital mass compensation through signal addition, and frequency domain analysis. The overall configuration of the test system is shown in Fig. 2.

Before carrying out accelerance measurements, we need to evaluate the force transducer and the accelerometer characteristics that are used in order to ensure that accurate amplitude and phase information can be obtained over the frequency range of interest. The accelerometer's sensitivity was determined by using the back-to-back calibration method. The calibration was performed with an exciter equipped with

a Kistler 808K reference accelerometer. Since this accelerometer is subjected to axial forces during the test, an extra mass effect was obtained as shown in Fig. 3. The calibration results are shown in Fig. 4 where it is clear that the effective frequency range of the Kistler 808T accelerometer for this test is limited to below 2500 Hz. Beyond 2500 Hz, the reference accelerometer's voltage sensitivity decreases seriously as frequency increases.

The force transducer was calibrated in the manner described by Dally, Riley and McConnell [2]. This method allows us to determine both the transducer's sensitivity and seismic mass at the same time. The calibration is performed by vibrating the force transducer at a constant acceleration level with a series of small masses attached. The actual force measured by the force transducer may be determined from Newton's second law where the mass is the sum of the attached mass and the transducer's seismic mass and the acceleration is that of the exciter table. The sensitivity and the seismic mass are extracted by plotting the weight of the added mass versus the ratio of the output voltages between the force transducer and the accelerometer. The data should plot as a straight line with the x-axis intercept occurring at the weight of the seismic mass and with the slope equal to the ratio of the force sensitivity to the acceleration sensitivity. All masses were determined by using a Mettler analytical balance accurate to 0.01 gram.

4. Procedure

(a) Excitation Method

Generally, excitation techniques are classified as one of five distinct types: steady state, random, periodic, transient and operating [3]. The steady–state type is typically a slowly swept sine or stepped sine sweep. In this work we used the stepped sine sweep excitation technique.

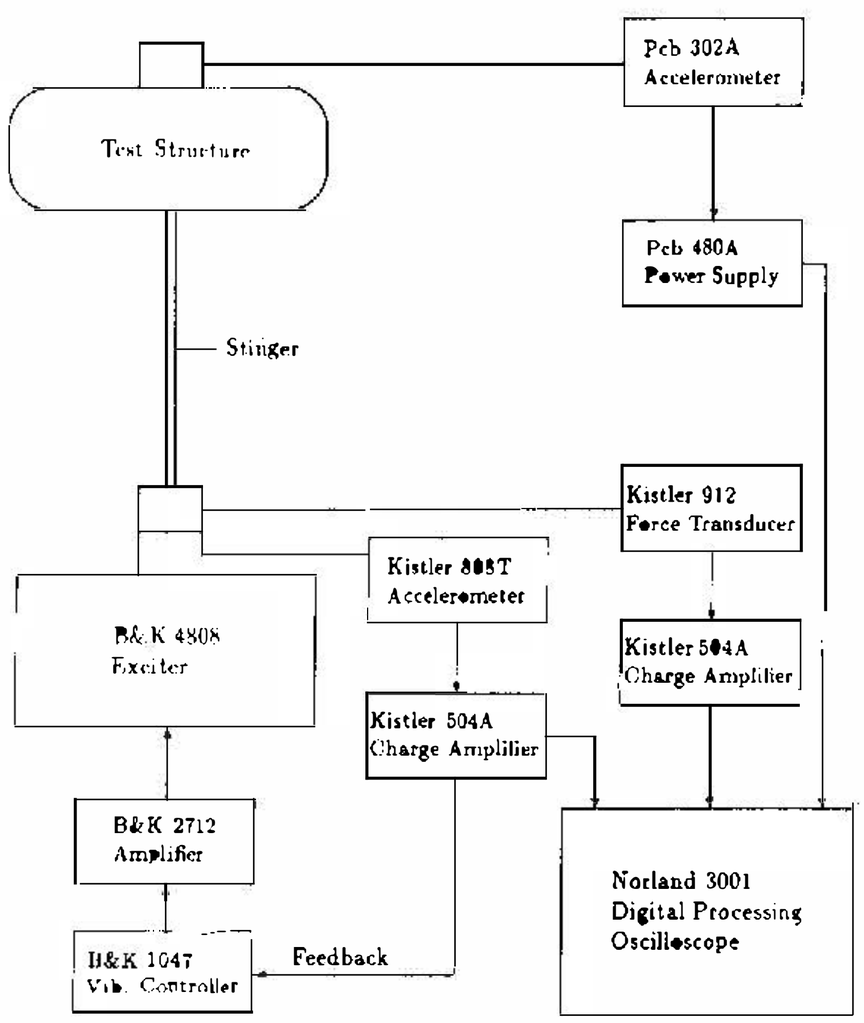

Fig. 2 Block diagram of instrumentation for tests with stinger

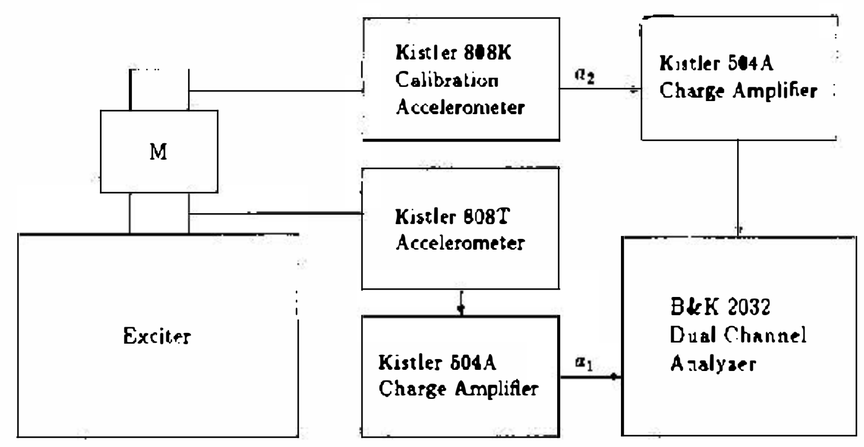

Fig. 3 Mass effect calibration of the Kistler 808T accelerometer

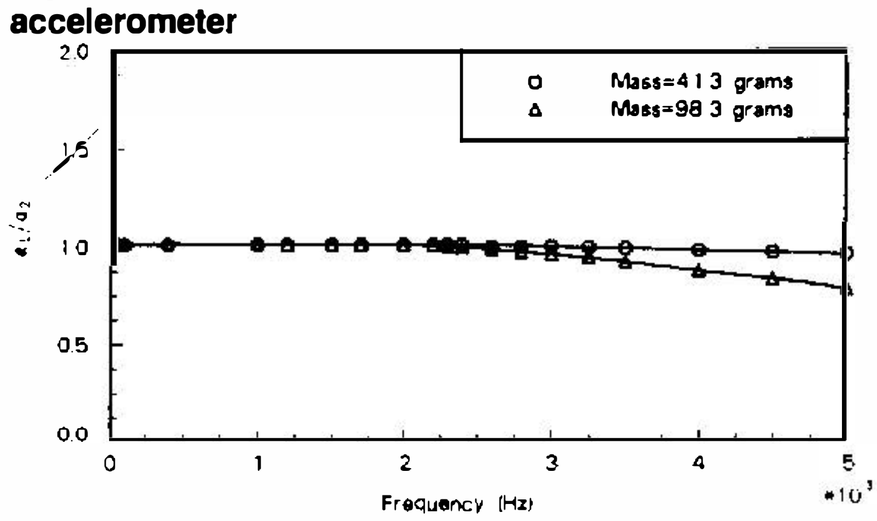

Fig. 4 Calibration curve of Kistler 808T accelerometer

In the stepped sine method, a constant magnitude sinusoidal excitation force is used at each test frequency. By "stepping" this sinusoidal signal through the frequency range of interest, the frequency response function can be evaluated for a number of discrete frequency points. At each frequency change, a delay is executed before signal analysis begins so that the structure has time to attain steady–state conditions.

(b) Evaluation of the Frequency Response Function

For each frequency to be analyzed, the following procedure is followed:

- The signal generator's output is adjusted to provide the desired frequency and base acceleration amplitude in the feedback controller.
- The transient response is allowed to die out.
- The mass compensation is implemented digitally by using Norland's signal manipulation capability.
- The frequency response function (FRF) is estimated at the selected test frequency by using Norland's computational capabilities.

The FRF value can be estimated directly from the time histories of the measured force (after mass compensation) and response acceleration signals. However, near resonance, the driving force is very small so that the time history of the force signal is seriously affected by noise. The noise could be low–frequency noise, electric line components, high–harmonic components of driving frequency caused by nonlinearities of either the exciter or the structure. The frequency domain analysis is necessary to isolate the structure's driving force signal from these noise contributions.

The frequency domain analysis consists of four steps. First, the mean square spectral density (MSSD) of the acceleration and corrected force signals are obtained. Second, an integration algorithm is used to determine the area under each frequency spectrum peak in order to obtain the signal's mean square for that frequency component. Third, the root mean square (RMS) values of the frequency component are determined by taking the square root of the mean square values. Fourth, the magnitude of accelerance at each discrete frequency is then obtained by taking the ratio of the RMS of output signal (acceleration) to the RMS of input signal (corrected force). This procedure is repeated three times on different data sets in order to reduce noise and random measurement error. A Hanning window is used to reduce digital filter leakage problems.

(c) Rigid Mass Test Specimen

The first test used a 0.535 lb rigid mass specimen. The reason for selecting a mass specimen is that its accelerance is a constant value of $1/M$ so that the experimental results using different test methods can be compared directly. Once it was shown that the new mass compensation method had promise, a more complex structure was tested. The experimental setup is shown in Fig. 5. A 0.15 in. diameter by 3. 85 in. long brass rod that weighed 0.023 lb was used as the stinger. The compensation mass on the stinger's exciter end includes the force transducer's seismic mass and mounting hardware mass. For this case, m_1 is around 0.017 lb. The compensated mass on the stinger's structure end m_2 is around 0.063 lb, which includes accelerometer 2 mass and mounting hardware mass. A set of individual discrete-frequency sinusoidal excitation forces was applied to the test mass. The vibration level was controlled to give a constant magnitude sinusoidal acceleration of the exciter table. The force transducer and accelerometer output signals (F_m, a_1, a_2) were connected to the data input channels of the Norland 3001 for on-line digital data acquisition and analysis. In order to estimate the force delivered to the structure, appropriately scaled acceleration signals were digitally subtracted from the force signal. The Norland 3001 was programmed

to gather the data, perform force compensation on the basis of different combinations of accelerations, and analyze the frequency components of the input and output signals. The measured accelerance frequency response functions were normalized by the mass's accelerance of 1/M. Any deviation from unity in these equations means that measurement error occurred.

(d) Beam Specimen Test

A rectangular aluminum double-cantilever beam with a central clamping mass was chosen as the second test structure as shown in Fig. 6. When this beam specimen is excited at its midpoint by a vibration exciter, the resulting dynamic system is equivalent to two cantilever beams of equal length being excited by base motion. If the cantilever beams are dynamically equal, the balanced structure causes no tipping imbalance of the exciter head.

Two experiments were performed on this beam specimen. First, the beam was driven directly at its midpoint by the electrodynamic vibration exciter as shown in Fig. 7(a). The driving force and driving point acceleration were recorded simultaneously by the Norland 3001. The measured driving point accelerance is normalized by $1/m_b$ where m_b is the single cantilever beam mass so that the dimensionless accelerance is given by $H(\omega)/(1/m_b)=(m_b a_2)/F_m$. This normalized accelerance is used as the reference against which the accelerances obtained through various stinger mass compensation techniques are to be compared.

In the second test, the beam specimen was driven through a 0.15 in. diameter, 3. 8 in. long steel rod as shown in Fig. 7(b). The masses that needed to be compensated for on the stinger's exciter end and stinger's structure end were around 0.144 lb and 0.081 lb, respectively. The stinger's mass was around 0.022 lb. The driving force was obtained from the force transducer that was mounted on the exciter end of the stinger. The effective inertia loading between the load cell and the structure was corrected on the basis of a_1 alone, a_2 alone, and a_1 and a_2 together. This compensation was done digitally by the Norland 3001.

Because the beam specimen is a multiresonant structure, the excitation frequency step size is controlled to achieve the required frequency resolution. Fine resolution is required in the vicinity of resonances and antiresonances of the beam in order to obtain accurate information for calculating natural frequency and structural damping. For frequencies outside the range of ±10% of a resonant or antiresonant frequency, large frequency increments were used. Since the aluminum beam is a lightly damped structure, its accelerance has a dynamic range that covers more than 80 dB over the test's frequency range. Systematic checks are made on the exciter table's acceleration levels in order to avoid amplifier saturation. To increase the usable dynamic range, we reduced the shaker table acceleration in the vicinity of each antiresonant

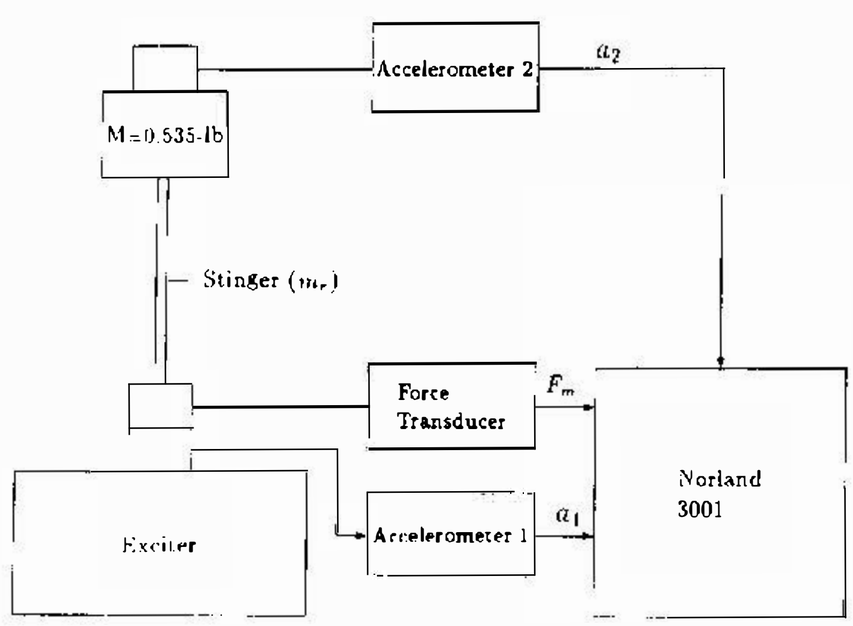

Fig. 5 Mass specimen measurement setup

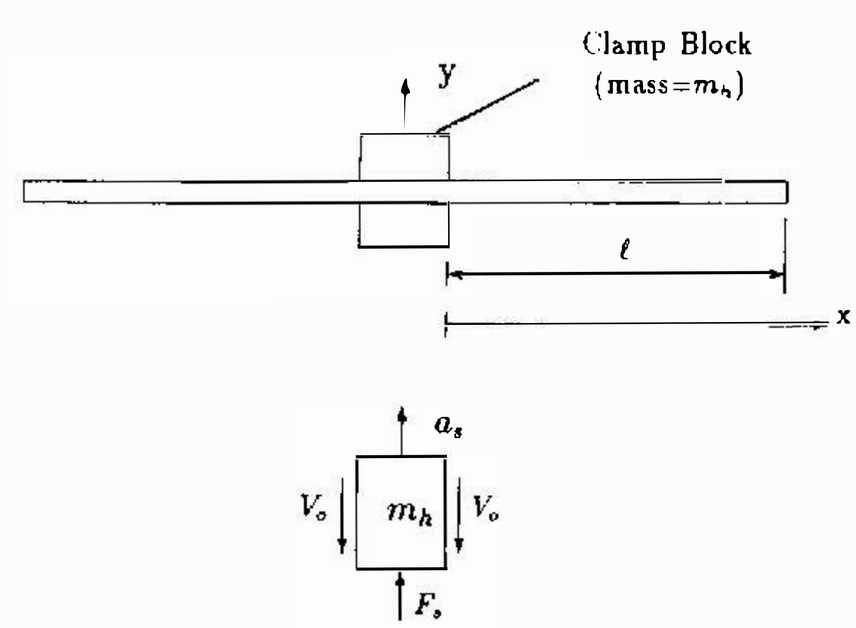

Fig. 6 Double cantilever beam specimen

frequency. In the vicinity of each resonant frequency the exciting force becomes very small since only the structure's damping force needs to be overcome. Accurately measuring the small resonant driving force is difficult because of the measurement system's noise floor. Frequency domain analysis was performed to isolate the force components from the system's noise. The tests included the beam's first four modes.

5. Results

(a) Rigid Mass Specimen

The various accelerance results obtained from the first experiment on rigid mass M are shown in Fig. 8. The measured normalization accelerances H_{c1}, H_{c2} and H_{c12}, are plotted against the frequency. The theoretical accelerances from Ref. [1] are also plotted in the same figure for direct comparison.

Figure 8 shows good agreement between experiment and theory, particularly for frequencies below 2500 Hz. Beyond 2500 Hz, the differences between the experimental and the theoretical results for H_{c1} and H_{c12} become larger and larger with increasing test frequency while H_{c2} is in much closer agreement. This trend can be explained by the mass loading effect of accelerometer a_1. The acceleration calibration curve (see Fig. 4) shows that there is a significant decrease in the accelerometer's voltage sensitivity (mv/g) beyond 2500 Hz when it has a mass loading. So the output signal voltage of accelerometer 1 becomes smaller than it should be. The denominators of Eqs. (2) and (6) involve acceleration a_1 and measured force F_m. We note that F_m and a_1 are 180° out of phase so that the measured values of H_{c1} and H_{c12} are above their corresponding theoretical curves for frequencies greater than 2500 Hz. The experimental results of H_{c2} are independent of a_1 so that no error is caused by the accelerometer's mass-loading effect.

Figure 8 shows that the three different mass compensation methods give nearly identical results in the lower frequency region below 1000 Hz. In high-frequency regions, the mass compensation based on the structure end or on the exciter end acceleration has a significant deviation from the correct value. The mass compensation based on both accelerations gives the best result, even for high frequencies. For example,

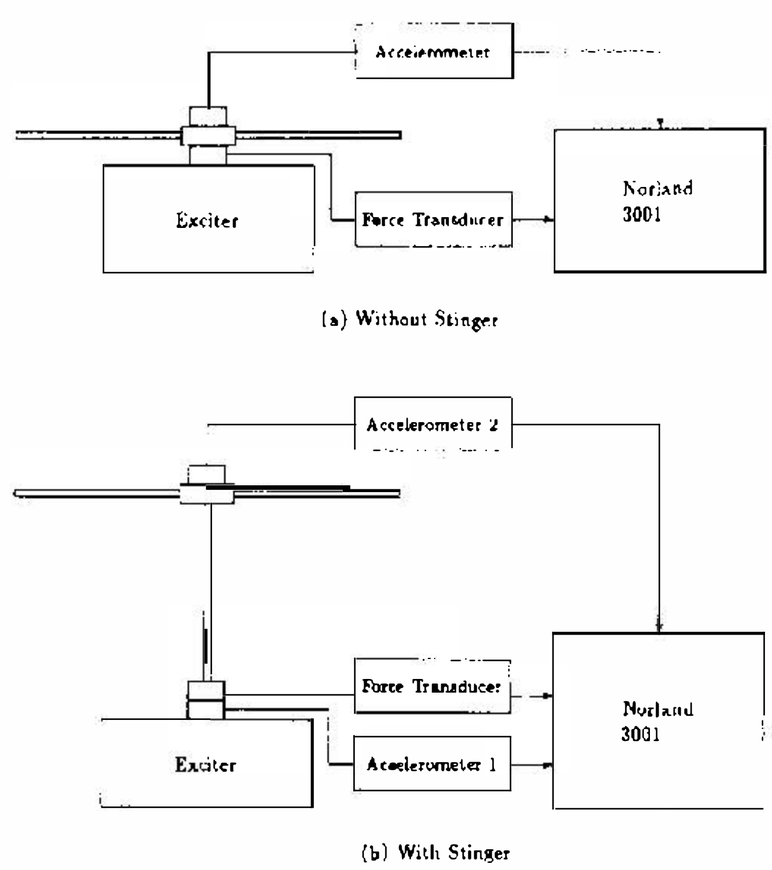

Fig. 7 Beam specimen measurement setup, (a) without stinger, (b) with Stinger

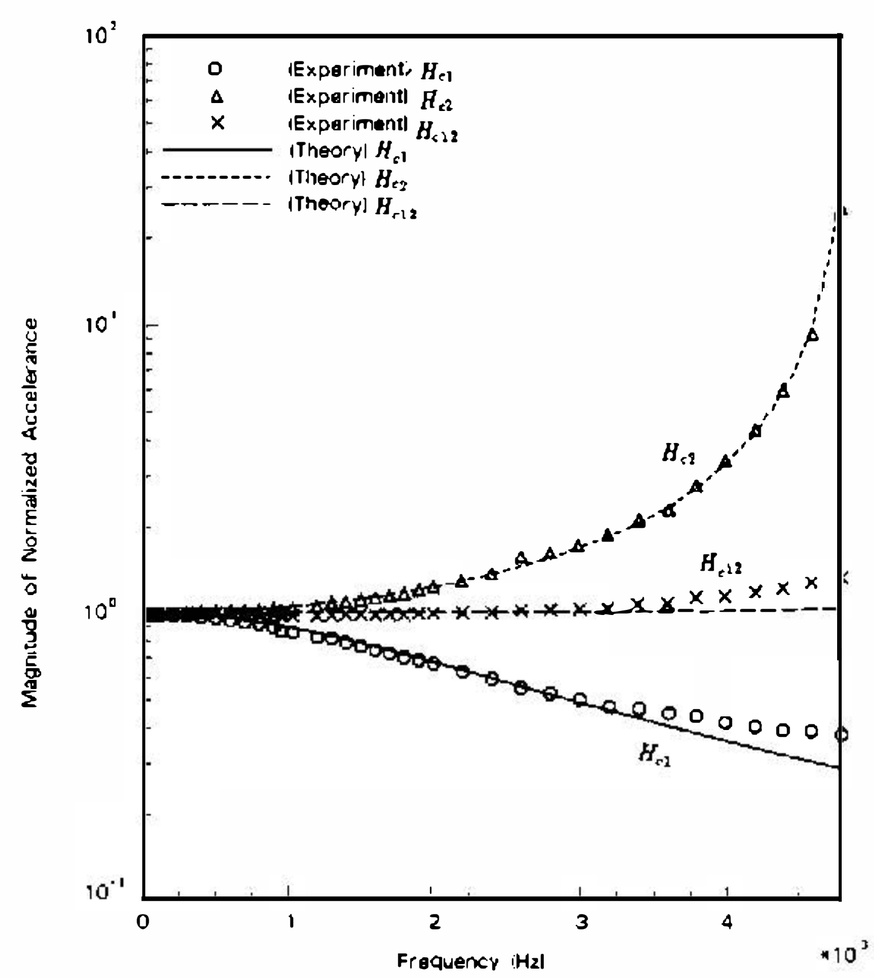

Fig. 8 Mass compensation experimental results compared with theory calculation: Mass specimen

in these experiments, with $f = 4000$ Hz, the errors are approximately 58% for H_{c1}, 237% for H_{c2}, but only 13. 6% for H_{c12}. The effectiveness of the new mass compensation method and the consequences of using only one acceleration (a_1 or a_2) are clearly demonstrated by this experiment.

(b) Beam Specimen

The results obtained from the beam specimen test are shown in Figs. 9-11. Each figure shows the normalized accelerance that corresponds to one of the mass compensation methods. In addition, the results obtained from the test without the stinger are plotted in each figure for comparison. Figures 9-11 show the same trends as those of the mass specimen experiment. For the first two modes, little difference exists among the three methods. However, at higher frequencies, $H_{c1}(\omega)$ gives an underestimation, $H_{c2}(\omega)$ an overestimation, and $H_{c12}(\omega)$ the best estimation of $H_s(\omega)$. These results are in agreement with the rigid mass trends.

Since the beam specimen is a multiresonant structure, a new experimental problem is encountered near the structure's resonant regions. Table 1 and Table 2 give detailed information on the beam experiments at the first four antiresonant and resonant frequencies.

Table 1 shows that the antiresonant frequencies are basically the same for all the three mass compensation methods as well as the reference values. Relatively small differences occur in the antiresonance magnitudes because in that region the structural forces are large and the structure's driving acceleration is small, requiring little force compensation.

Table 2 shows that the resonant frequencies predicted by H_{c1} shift to the left side of the reference values and shift to the right side if predicted by H_{c2}. H_{c12} gives the best estimation of the resonance frequency especially for the high modes. For example, near the fourth resonance mode, the resonant frequency from H_{c1} shifts to the left about 9 Hz; H_{c2} shifts around 40 Hz; and H_{c12} shifts only 2 Hz. The resonant frequency errors are caused by the high and low force levels that are used in the accelerance measurements because of the approximations used in the mass compensation processing.

Table 2 also shows poor results in predicting the resonant magnitudes when all three mass compensation methods are employed. These large measurement errors that occur near the specimen's resonant regions

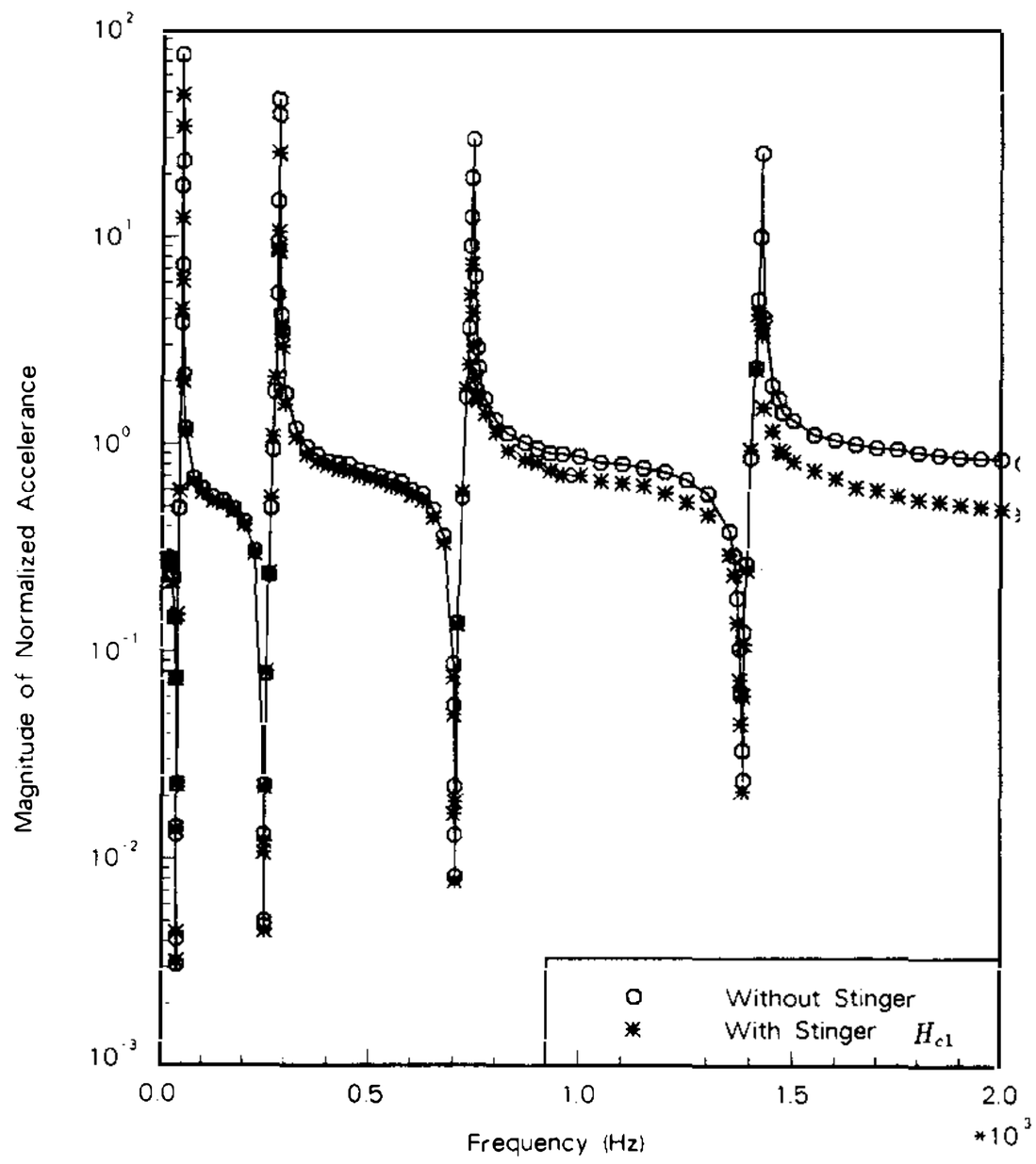

Fig. 9 Comparison of measured accelerance with and without stinger (mass compensation based on a_1): Beam specimen

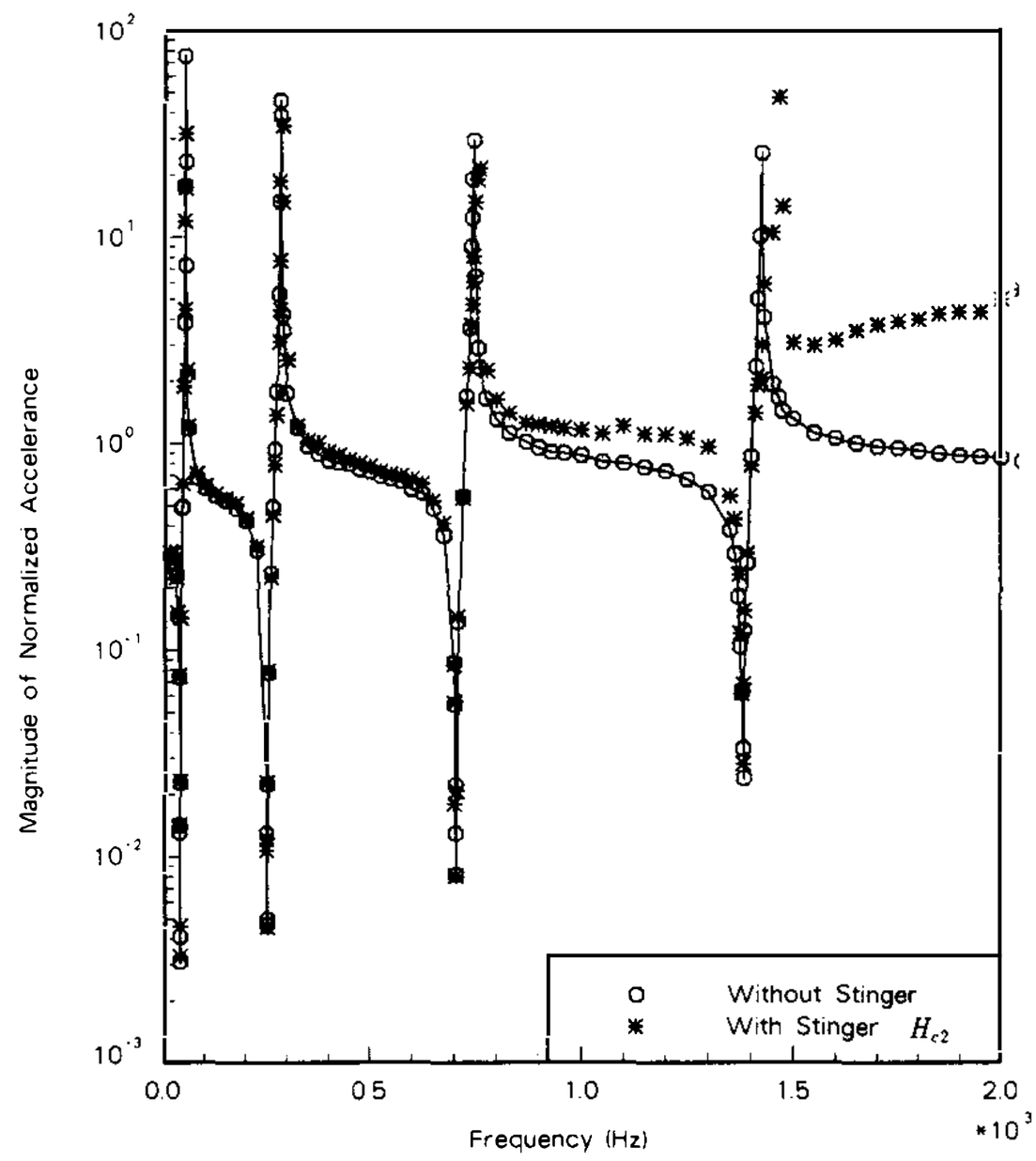

Fig. 10 Comparison of measured accelerance with and without stinger (mass compensation based on a_2): Beam specimen

TABLE 1 EXPERIMENTAL RESULTS OF THE FIRST FOUR ANTIRESONANT FREQUENCIES AND MAGNITUDES FOR THE BEAM SPECIMEN

FREQUENCY				
Mode	Without Stinger	With Stinger		
	$H_s(Hz)$	$H_{c1}(Hz)$	$H_{c2}(Hz)$	$H_{c12}(Hz)$
First	40.1	40.0	40.0	40.0
Second	252.1	251.8	251.9	251.8
Third	705.2	704.6	704.6	704.6
Fourth	1382.2	1380.9	1380.9	1380.9

MAGNITUDE				
Mode	Without Stinger	With Stinger		
	H_s	H_{c1}	H_{c2}	H_{c12}
First	0.0031	0.0032	0.0033	0.0032
Second	0.0047	0.0045	0.0049	0.0046
Third	0.0082	0.0078	0.0084	0.0081
Fourth	0.0240	0.0212	0.0282	0.00245

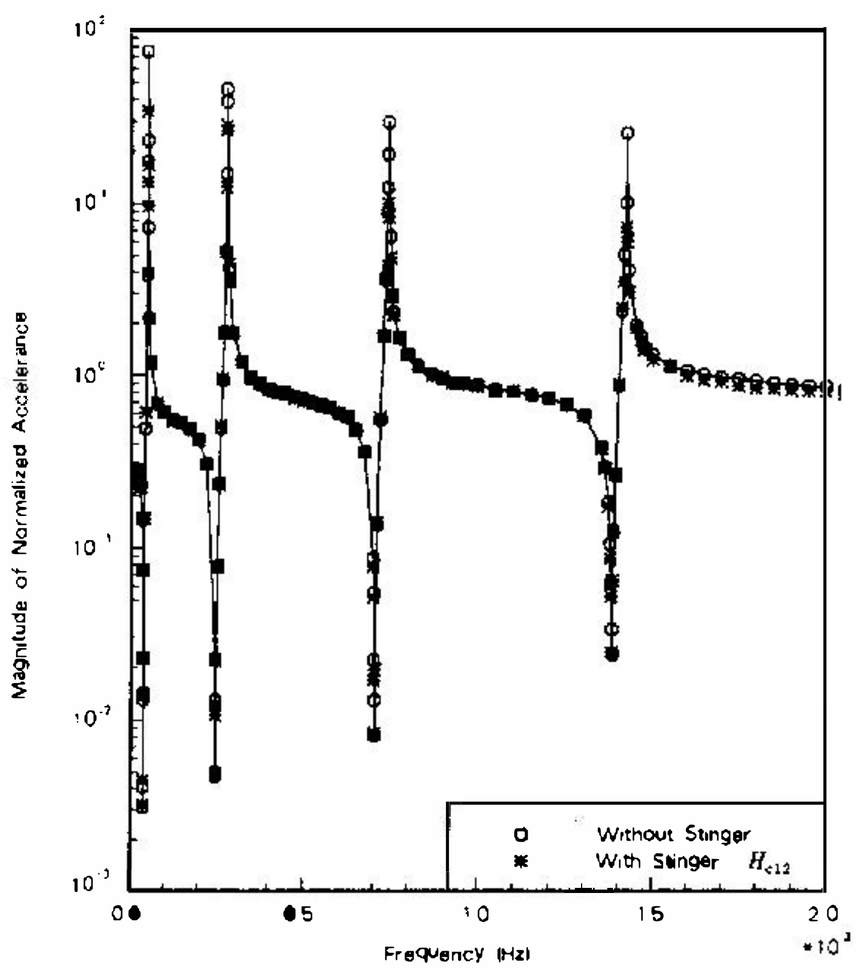

Fig. 11 Comparison of measured accelerance with and without stinger (mass compensation based on both a_1 and a_2): Beam specimen

TABLE 2 EXPERIMENTAL RESULTS OF THE FIRST FOUR RESONANT FREQUENCIES AND MAGNITUDES FOR THE BEAM SPECIMEN

FREQUENCY				
Mode	Without Stinger	With Stinger		
	$H_s(Hz)$	$H_{c1}(Hz)$	$H_{c2}(Hz)$	$H_{c12}(Hz)$
First	51.4	51.2 (0.4%)	52.2 (1.6%)	51.5 (0.2%)
Second	282.9	282.1 (0.3%)	288.4 (1.9%)	283.0 (0.04%)
Third	744.7	742.3 (0.3%)	758.1 (1.8%)	743.2 (0.2%)
Fourth	1424.3	1415.3 (0.6%)	1465.9 (2.9%)	1422.1 (0.15%)

MAGNITUDE				
Mode	Without Stinger	With Stinger		
	H_s	H_{c1}	H_{c2}	H_{c12}
First	75.30	48.34 (35.8%)	31.72 (57.9%)	34.44 (54.3%)
Second	45.72	25.46 (44.3%)	34.73 (24.0%)	28.33 (38.0%)
Third	29.46	7.31 (75.2%)	21.54 (26.9%)	10.03 (66.0%)
Fourth	26.49	4.22 (84.1%)	46.77 (76.6%)	7.19 (72.9%)

suggest that additional issues must be addressed. Although there exists an inherent measurement accuracy problem near the structural resonant regions, other reasons related to the mass compensation method may cause this error. Further investigation has been performed theoretically on the mass compensation procedure near the structure's resonant regions. This analysis shows that tremendous errors can occur for reasons that are unfamiliar to the experimental modal analysis community [4].

6. Conclusion

In order to reduce transducer rotational inertia loading on the structure under test, the force transducer can be removed to the stinger exciter end. The stinger mass compensation of this arrangement has been investigated experimentally. The results follow.

1. Because of the compliance of the stinger, mass compensation based on exciter–end acceleration will underestimate the structure's accelerance, while compensation based on the stinger's structure–end acceleration will overestimate the accelerance.
2. The mass compensation using two accelerations has been shown to improve the accuracy by a considerable degree. A significant advantage of the new method is the ability to predict FRF in the high–frequency region.
3. Experimental difficulties have been found in predicting the resonant magnitudes for all three mass compensation methods.

Acknowledgments

The authors wish to thank the Iowa State University Engineering Research Institute and the Department of Aerospace Engineering and Engineering Mechanics for support of this research.

References

[1] Hu, X.; McConnell, K. G. "Stinger Mass Compensation, Part One: Theoretical Study." *Int J Anal Exp Modal Anal* v 8 n 1 Jan 1993 p 35-44

[2] Dalley, J. W.; Riley, W. F.; McConnell, K. G. *Instrumentation for Engineering Measurements*. New York: John Wiley & Sons, Inc. ; 1976.

[3] Olsen, N. "Excitation Functions for Structural Frequency Response Measurements." *Proceedings of the 2nd International Modal Analysis Conference*, Orlando, FL, Feb 6-9, 1984. v 2 p 872–976

[4] Hu, X. ; McConnell, K. G. "Force Transducer Mass Compensation Can Cause Large FRF Errors at Resonance." *Proceedings of the 10th International Modal Analysis Conference*, San Diego, CA, Feb 3-7, 1992. v 2 p 1373-1379